MIT Open Access Articles

Measurements of the properties of Lambdac(2595), Lambdac(2625), Sigmac(2455), and Sigmac(2520) baryons

Measurements of the properties of $\Lambda_c(2595)$, $\Lambda_c(2625)$, $\Sigma_c(2455)$, and $\Sigma_c(2520)$ baryons

T. Aaltonen,[21] B. Álvarez González,[9,x] S. Amerio,[41a] D. Amidei,[32] A. Anastassov,[36] A. Annovi,[17] J. Antos,[12]
G. Apollinari,[15] J. A. Appel,[15] A. Apresyan,[46] T. Arisawa,[56] A. Artikov,[13] J. Asaadi,[51] W. Ashmanskas,[15] B. Auerbach,[59]
A. Aurisano,[51] F. Azfar,[40] W. Badgett,[15] A. Barbaro-Galtieri,[26] V. E. Barnes,[46] B. A. Barnett,[23] P. Barria,[44c,44a] P. Bartos,[12]
M. Bauce,[41b,41a] G. Bauer,[30] F. Bedeschi,[44a] D. Beecher,[28] S. Behari,[23] G. Bellettini,[44b,44a] J. Bellinger,[58] D. Benjamin,[14]
A. Beretvas,[15] A. Bhatti,[48] M. Binkley,[15,a] D. Bisello,[41b,41a] I. Bizjak,[28,cc] K. R. Bland,[5] B. Blumenfeld,[23] A. Bocci,[14]
A. Bodek,[47] D. Bortoletto,[46] J. Boudreau,[45] A. Boveia,[11] B. Brau,[15,b] L. Brigliadori,[6b,6a] A. Brisuda,[12] C. Bromberg,[33]
E. Brucken,[21] M. Bucciantonio,[44b,44a] J. Budagov,[13] H. S. Budd,[47] S. Budd,[22] K. Burkett,[15] G. Busetto,[41b,41a] P. Bussey,[19]
A. Buzatu,[31] C. Calancha,[29] S. Camarda,[4] M. Campanelli,[33] M. Campbell,[32] F. Canelli,[11,15] B. Carls,[22] D. Carlsmith,[58]
R. Carosi,[44a] S. Carrillo,[16,l] S. Carron,[15] B. Casal,[9] M. Casarsa,[15] A. Castro,[6b,6a] P. Catastini,[20] D. Cauz,[52a] V. Cavaliere,[22]
M. Cavalli-Sforza,[4] A. Cerri,[26,g] L. Cerrito,[28,r] Y. C. Chen,[1] M. Chertok,[7] G. Chiarelli,[44a] G. Chlachidze,[15] F. Chlebana,[15]
K. Cho,[25] D. Chokheli,[13] J. P. Chou,[20] W. H. Chung,[58] Y. S. Chung,[47] C. I. Ciobanu,[42] M. A. Ciocci,[44c,44a] A. Clark,[18]
C. Clarke,[57] G. Compostella,[41b,41a] M. E. Convery,[15] J. Conway,[7] M. Corbo,[42] M. Cordelli,[17] C. A. Cox,[7] D. J. Cox,[7]
F. Crescioli,[44b,44a] C. Cuenca Almenar,[59] J. Cuevas,[9,x] R. Culbertson,[15] D. Dagenhart,[15] N. d'Ascenzo,[42,v] M. Datta,[15]
P. de Barbaro,[47] S. De Cecco,[49a] G. De Lorenzo,[4] M. Dell'Orso,[44b,44a] C. Deluca,[4] L. Demortier,[48] J. Deng,[14,d]
M. Deninno,[6a] F. Devoto,[21] M. d'Errico,[41b,41a] A. Di Canto,[44b,44a] B. Di Ruzza,[44a] J. R. Dittmann,[5] M. D'Onofrio,[27]
S. Donati,[44b,44a] P. Dong,[15] M. Dorigo,[52a] T. Dorigo,[41a] K. Ebina,[56] A. Elagin,[51] A. Eppig,[32] R. Erbacher,[7] D. Errede,[22]
S. Errede,[22] N. Ershaidat,[42,aa] R. Eusebi,[51] H. C. Fang,[26] S. Farrington,[40] M. Feindt,[24] J. P. Fernandez,[29] C. Ferrazza,[44d,44a]
R. Field,[16] G. Flanagan,[46,t] R. Forrest,[7] M. J. Frank,[5] M. Franklin,[20] J. C. Freeman,[15] Y. Funakoshi,[56] I. Furic,[16]
M. Gallinaro,[48] J. Galyardt,[10] J. E. Garcia,[18] A. F. Garfinkel,[46] P. Garosi,[44c,44a] H. Gerberich,[22] E. Gerchtein,[15]
S. Giagu,[49b,49a] V. Giakoumopoulou,[3] P. Giannetti,[44a] K. Gibson,[45] C. M. Ginsburg,[15] N. Giokaris,[3] P. Giromini,[17]
M. Giunta,[44a] G. Giurgiu,[23] V. Glagolev,[13] D. Glenzinski,[15] M. Gold,[35] D. Goldin,[51] N. Goldschmidt,[16] A. Golossanov,[15]
G. Gomez,[9] G. Gomez-Ceballos,[30] M. Goncharov,[30] O. González,[29] I. Gorelov,[35] A. T. Goshaw,[14] K. Goulianos,[48]
S. Grinstein,[4] C. Grosso-Pilcher,[11] R. C. Group,[55,15] J. Guimaraes da Costa,[20] Z. Gunay-Unalan,[33] C. Haber,[26]
S. R. Hahn,[15] E. Halkiadakis,[50] A. Hamaguchi,[39] J. Y. Han,[47] F. Happacher,[17] K. Hara,[53] D. Hare,[50] M. Hare,[54] R. F. Harr,[57]
K. Hatakeyama,[5] C. Hays,[40] M. Heck,[24] J. Heinrich,[43] M. Herndon,[58] S. Hewamanage,[5] D. Hidas,[50] A. Hocker,[15]
W. Hopkins,[15,h] D. Horn,[24] S. Hou,[1] R. E. Hughes,[37] M. Hurwitz,[11] U. Husemann,[59] N. Hussain,[31] M. Hussein,[33]
J. Huston,[33] G. Introzzi,[44a] M. Iori,[49b,49a] A. Ivanov,[7,p] E. James,[15] D. Jang,[10] B. Jayatilaka,[14] E. J. Jeon,[25] M. K. Jha,[6a]
S. Jindariani,[15] W. Johnson,[7] M. Jones,[46] K. K. Joo,[25] S. Y. Jun,[10] T. R. Junk,[15] T. Kamon,[51] P. E. Karchin,[57] A. Kasmi,[5]
Y. Kato,[39,o] W. Ketchum,[11] J. Keung,[43] V. Khotilovich,[51] B. Kilminster,[15] D. H. Kim,[25] H. S. Kim,[25] H. W. Kim,[25]
J. E. Kim,[25] M. J. Kim,[17] S. B. Kim,[25] S. H. Kim,[53] Y. K. Kim,[11] N. Kimura,[56] M. Kirby,[15] S. Klimenko,[16] K. Kondo,[56]
D. J. Kong,[25] J. Konigsberg,[16] A. V. Kotwal,[14] M. Kreps,[24,bb] J. Kroll,[43] D. Krop,[11] N. Krumnack,[5,m] M. Kruse,[14]
V. Krutelyov,[51,e] T. Kuhr,[24] M. Kurata,[53] S. Kwang,[11] A. T. Laasanen,[46] S. Lami,[44a] S. Lammel,[15] M. Lancaster,[28]
R. L. Lander,[7] K. Lannon,[37,w] A. Lath,[50] G. Latino,[44b,44a] T. LeCompte,[2] E. Lee,[51] H. S. Lee,[11] J. S. Lee,[25] S. W. Lee,[51,y]
S. Leo,[44b,44a] S. Leone,[44a] J. D. Lewis,[15] C.-J. Lin,[26] J. Linacre,[40] M. Lindgren,[15] E. Lipeles,[43] A. Lister,[18]
D. O. Litvintsev,[15] C. Liu,[45] Q. Liu,[46] T. Liu,[15] S. Lockwitz,[59] A. Loginov,[59] D. Lucchesi,[41b,41a] J. Lueck,[24] P. Lujan,[26]
P. Lukens,[15] G. Lungu,[48] J. Lys,[26] R. Lysak,[12] R. Madrak,[15] K. Maeshima,[15] K. Makhoul,[30] S. Malik,[48] G. Manca,[27,c]
A. Manousakis-Katsikakis,[3] F. Margaroli,[46] C. Marino,[24] M. Martínez,[4] R. Martínez-Ballarín,[29] P. Mastrandrea,[49a]
M. E. Mattson,[57] P. Mazzanti,[6a] K. S. McFarland,[47] P. McIntyre,[51] R. McNulty,[27,j] A. Mehta,[27] P. Mehtala,[21]
A. Menzione,[44a] C. Mesropian,[48] T. Miao,[15] D. Mietlicki,[32] A. Mitra,[1] H. Miyake,[53] S. Moed,[20] N. Moggi,[6a]
M. N. Mondragon,[15,l] C. S. Moon,[25] R. Moore,[15] M. J. Morello,[15] J. Morlock,[24] P. Movilla Fernandez,[15] A. Mukherjee,[15]
Th. Muller,[24] P. Murat,[15] M. Mussini,[6b,6a] J. Nachtman,[15,n] Y. Nagai,[53] J. Naganoma,[56] I. Nakano,[38] A. Napier,[54] J. Nett,[51]
C. Neu,[60] M. S. Neubauer,[22] J. Nielsen,[26,f] L. Nodulman,[2] O. Norniella,[22] E. Nurse,[28] L. Oakes,[40] S. H. Oh,[14] Y. D. Oh,[25]
I. Oksuzian,[60] T. Okusawa,[39] R. Orava,[21] L. Ortolan,[4] S. Pagan Griso,[41b,41a] C. Pagliarone,[52a] E. Palencia,[9,g]
V. Papadimitriou,[15] A. A. Paramonov,[2] J. Patrick,[15] G. Pauletta,[52b,52a] M. Paulini,[10] C. Paus,[30] D. E. Pellett,[7] A. Penzo,[52a]
T. J. Phillips,[14] G. Piacentino,[44a] E. Pianori,[43] J. Pilot,[37] K. Pitts,[22] C. Plager,[8] L. Pondrom,[58] K. Potamianos,[46]
O. Poukhov,[13,a] F. Prokoshin,[13,z] A. Pronko,[15] F. Ptohos,[17,i] E. Pueschel,[10] G. Punzi,[44b,44a] J. Pursley,[58] A. Rahaman,[45]
V. Ramakrishnan,[58] N. Ranjan,[46] I. Redondo,[29] P. Renton,[40] M. Rescigno,[49a] T. Riddick,[28] F. Rimondi,[6b,6a] L. Ristori,[45,15]
A. Robson,[19] T. Rodrigo,[9] T. Rodriguez,[43] E. Rogers,[22] S. Rolli,[54] R. Roser,[15] M. Rossi,[52a] F. Rubbo,[15] F. Ruffini,[44c,44a]
A. Ruiz,[9] J. Russ,[10] V. Rusu,[15] A. Safonov,[51] W. K. Sakumoto,[47] Y. Sakurai,[56] L. Santi,[52b,52a] L. Sartori,[44a] K. Sato,[53]

V. Saveliev,[42,v] A. Savoy-Navarro,[42] P. Schlabach,[15] A. Schmidt,[24] E. E. Schmidt,[15] M. P. Schmidt,[59,a] M. Schmitt,[36] T. Schwarz,[7] L. Scodellaro,[9] A. Scribano,[44c,44a] F. Scuri,[44a] A. Sedov,[46] S. Seidel,[35] Y. Seiya,[39] A. Semenov,[13] F. Sforza,[44b,44a] A. Sfyrla,[22] S. Z. Shalhout,[7] T. Shears,[27] P. F. Shepard,[45] M. Shimojima,[53,u] S. Shiraishi,[11] M. Shochet,[11] I. Shreyber,[34] A. Simonenko,[13] P. Sinervo,[31] A. Sissakian,[13,a] K. Sliwa,[54] J. R. Smith,[7] F. D. Snider,[15] A. Soha,[15] S. Somalwar,[50] V. Sorin,[4] P. Squillacioti,[15] M. Stancari,[15] M. Stanitzki,[59] R. St. Denis,[19] B. Stelzer,[31] O. Stelzer-Chilton,[31] D. Stentz,[36] J. Strologas,[35] G. L. Strycker,[32] Y. Sudo,[53] A. Sukhanov,[16] I. Suslov,[13] K. Takemasa,[53] Y. Takeuchi,[53] J. Tang,[11] M. Tecchio,[32] P. K. Teng,[1] J. Thom,[15,h] J. Thome,[10] G. A. Thompson,[22] E. Thomson,[43] P. Ttito-Guzmán,[29] S. Tkaczyk,[15] D. Toback,[51] S. Tokar,[12] K. Tollefson,[33] T. Tomura,[53] D. Tonelli,[15] S. Torre,[17] D. Torretta,[15] P. Totaro,[41a] M. Trovato,[44d,44a] Y. Tu,[43] F. Ukegawa,[53] S. Uozumi,[25] A. Varganov,[32] F. Vázquez,[16,l] G. Velev,[15] C. Vellidis,[3] M. Vidal,[29] I. Vila,[9] R. Vilar,[9] J. Vizán,[9] M. Vogel,[35] G. Volpi,[44b,44a] P. Wagner,[43] R. L. Wagner,[15] T. Wakisaka,[39] R. Wallny,[8] S. M. Wang,[1] A. Warburton,[31] D. Waters,[28] M. Weinberger,[51] W. C. Wester III,[15] B. Whitehouse,[54] D. Whiteson,[43,d] A. B. Wicklund,[2] E. Wicklund,[15] S. Wilbur,[11] F. Wick,[24] H. H. Williams,[43] J. S. Wilson,[37] P. Wilson,[15] B. L. Winer,[37] P. Wittich,[15,h] S. Wolbers,[15] H. Wolfe,[37] T. Wright,[32] X. Wu,[18] Z. Wu,[5] K. Yamamoto,[39] J. Yamaoka,[14] T. Yang,[15] U. K. Yang,[11,q] Y. C. Yang,[25] W.-M. Yao,[26] G. P. Yeh,[15] K. Yi,[15,n] J. Yoh,[15] K. Yorita,[56] T. Yoshida,[39,k] G. B. Yu,[14] I. Yu,[25] S. S. Yu,[15] J. C. Yun,[15] A. Zanetti,[52a] Y. Zeng,[14] and S. Zucchelli[6b,6a]

(CDF Collaboration)

[1]*Institute of Physics, Academia Sinica, Taipei, Taiwan 11529, Republic of China*
[2]*Argonne National Laboratory, Argonne, Illinois 60439, USA*
[3]*University of Athens, 157 71 Athens, Greece*
[4]*Institut de Fisica d'Altes Energies, ICREA, Universitat Autonoma de Barcelona, E-08193, Bellaterra (Barcelona), Spain*
[5]*Baylor University, Waco, Texas 76798, USA*
[6a]*Istituto Nazionale di Fisica Nucleare Bologna, I-40127 Bologna, Italy*
[6b]*University of Bologna, I-40127 Bologna, Italy*
[7]*University of California, Davis, Davis, California 95616, USA*
[8]*University of California, Los Angeles, Los Angeles, California 90024, USA*
[9]*Instituto de Fisica de Cantabria, CSIC-University of Cantabria, 39005 Santander, Spain*
[10]*Carnegie Mellon University, Pittsburgh, Pennsylvania 15213, USA*
[11]*Enrico Fermi Institute, University of Chicago, Chicago, Illinois 60637, USA*
[12]*Comenius University, 842 48 Bratislava, Slovakia; Institute of Experimental Physics, 040 01 Kosice, Slovakia*
[13]*Joint Institute for Nuclear Research, RU-141980 Dubna, Russia*
[14]*Duke University, Durham, North Carolina 27708, USA*
[15]*Fermi National Accelerator Laboratory, Batavia, Illinois 60510, USA*
[16]*University of Florida, Gainesville, Florida 32611, USA*
[17]*Laboratori Nazionali di Frascati, Istituto Nazionale di Fisica Nucleare, I-00044 Frascati, Italy*
[18]*University of Geneva, CH-1211 Geneva 4, Switzerland*
[19]*Glasgow University, Glasgow G12 8QQ, United Kingdom*
[20]*Harvard University, Cambridge, Massachusetts 02138, USA*
[21]*Division of High Energy Physics, Department of Physics, University of Helsinki and Helsinki Institute of Physics, FIN-00014, Helsinki, Finland*
[22]*University of Illinois, Urbana, Illinois 61801, USA*
[23]*The Johns Hopkins University, Baltimore, Maryland 21218, USA*
[24]*Institut für Experimentelle Kernphysik, Karlsruhe Institute of Technology, D-76131 Karlsruhe, Germany*
[25]*Center for High Energy Physics: Kyungpook National University, Daegu 702-701, Korea; Seoul National University, Seoul 151-742, Korea; Sungkyunkwan University, Suwon 440-746, Korea; Korea Institute of Science and Technology Information, Daejeon 305-806, Korea; Chonnam National University, Gwangju 500-757, Korea; Chonbuk National University, Jeonju 561-756, Korea*
[26]*Ernest Orlando Lawrence Berkeley National Laboratory, Berkeley, California 94720, USA*
[27]*University of Liverpool, Liverpool L69 7ZE, United Kingdom*
[28]*University College London, London WC1E 6BT, United Kingdom*
[29]*Centro de Investigaciones Energeticas Medioambientales y Tecnologicas, E-28040 Madrid, Spain*
[30]*Massachusetts Institute of Technology, Cambridge, Massachusetts 02139, USA*
[31]*Institute of Particle Physics: McGill University, Montréal, Québec, Canada H3A 2T8; Simon Fraser University, Burnaby, British Columbia, Canada V5A 1S6; University of Toronto, Toronto, Ontario, Canada M5S 1A7; and TRIUMF, Vancouver, British Columbia, Canada V6T 2A3*

[32]University of Michigan, Ann Arbor, Michigan 48109, USA

[33]Michigan State University, East Lansing, Michigan 48824, USA

[34]Institution for Theoretical and Experimental Physics, ITEP, Moscow 117259, Russia

[35]University of New Mexico, Albuquerque, New Mexico 87131, USA

[36]Northwestern University, Evanston, Illinois 60208, USA

[37]The Ohio State University, Columbus, Ohio 43210, USA

[38]Okayama University, Okayama 700-8530, Japan

[39]Osaka City University, Osaka 588, Japan

[40]University of Oxford, Oxford OX1 3RH, United Kingdom

[41a]Istituto Nazionale di Fisica Nucleare, Sezione di Padova-Trento, I-35131 Padova, Italy

[41b]University of Padova, I-35131 Padova, Italy

[42]LPNHE, Universite Pierre et Marie Curie/IN2P3-CNRS, UMR7585, Paris, F-75252 France

[43]University of Pennsylvania, Philadelphia, Pennsylvania 19104, USA

[44a]Istituto Nazionale di Fisica Nucleare Pisa, I-56127 Pisa, Italy

[44b]University of Pisa, I-56127 Pisa, Italy

[44c]University of Siena, I-56127 Pisa, Italy

[44d]Scuola Normale Superiore, I-56127 Pisa, Italy

[45]University of Pittsburgh, Pittsburgh, Pennsylvania 15260, USA

[46]Purdue University, West Lafayette, Indiana 47907, USA

[47]University of Rochester, Rochester, New York 14627, USA

[48]The Rockefeller University, New York, New York 10065, USA

[49a]Istituto Nazionale di Fisica Nucleare, Sezione di Roma 1, I-00185 Roma, Italy

[49b]Sapienza Università di Roma, I-00185 Roma, Italy

[50]Rutgers University, Piscataway, New Jersey 08855, USA

[51]Texas A&M University, College Station, Texas 77843, USA

[52a]Istituto Nazionale di Fisica Nucleare Trieste/Udine, I-34100 Trieste, Italy

[52b]University of Udine, I-33100 Udine, Italy

[53]University of Tsukuba, Tsukuba, Ibaraki 305, Japan

[54]Tufts University, Medford, Massachusetts 02155, USA

[55]University of Virginia, Charlottesville, Virginia 22906, USA

[56]Waseda University, Tokyo 169, Japan

[57]Wayne State University, Detroit, Michigan 48201, USA

[58]University of Wisconsin, Madison, Wisconsin 53706, USA

[a]Deceased

[b]With visitor from University of Massachusetts Amherst, Amherst, MA 01003, USA

[c]With visitor from Istituto Nazionale di Fisica Nucleare, Sezione di Cagliari, 09042 Monserrato (Cagliari), Italy

[d]With visitor from University of California, Irvine, Irvine, CA 92697, USA

[e]With visitor from University of California, Santa Barbara, Santa Barbara, CA 93106, USA

[f]With visitor from University of California, Santa Cruz, Santa Cruz, CA 95064, USA

[g]With visitor from CERN,CH-1211 Geneva, Switzerland

[h]With visitor from Cornell University, Ithaca, NY 14853, USA

[i]With visitor from University of Cyprus, Nicosia CY-1678, Cyprus

[j]With visitor from University College Dublin, Dublin 4, Ireland

[k]With visitor from University of Fukui, Fukui City, Fukui Prefecture, Japan 910-0017

[l]With visitor from Universidad Iberoamericana, Mexico D.F., Mexico

[m]With visitor from Iowa State University, Ames, IA 50011, USA

[n]With visitor from University of Iowa, Iowa City, IA 52242, USA

[o]With visitor from Kinki University, Higashi-Osaka City, Japan 577-8502

[p]With visitor from Kansas State University, Manhattan, KS 66506, USA

[q]With visitor from University of Manchester, Manchester M13 9PL, United Kingdom

[r]With visitor from Queen Mary, University of London, London, E1 4NS, United Kingdom

[s]With visitor from University of Melbourne, Victoria 3010, Australia

[t]With visitor from Muons, Inc., Batavia, IL 60510, USA

[u]With visitor from Nagasaki Institute of Applied Science, Nagasaki, Japan

[v]With visitor from National Research Nuclear University, Moscow, Russia

[w]With visitor from University of Notre Dame, Notre Dame, IN 46556, USA

[x]With visitor from Universidad de Oviedo, E-33007 Oviedo, Spain

[y]With visitor from Texas Tech University, Lubbock, TX 79609, USA

[z]With visitor from Universidad Tecnica Federico Santa Maria, 110v Valparaiso, Chile

[aa]With visitor from Yarmouk University, Irbid 211-63, Jordan

[bb]With visitor from University of Warwick, Coventry CV4 7AL, United Kingdom

[cc]On leave from J. Stefan Institute, Ljubljana, Slovenia

[59]*Yale University, New Haven, Connecticut 06520, USA*
[60]*University of Virginia, Charlottesville, Virginia 22906, USA*

We report measurements of the resonance properties of $\Lambda_c(2595)^+$ and $\Lambda_c(2625)^+$ baryons in their decays to $\Lambda_c^+ \pi^+ \pi^-$ as well as $\Sigma_c(2455)^{++,0}$ and $\Sigma_c(2520)^{++,0}$ baryons in their decays to $\Lambda_c^+ \pi^\pm$ final states. These measurements are performed using data corresponding to 5.2 fb^{-1} of integrated luminosity from $p\bar{p}$ collisions at $\sqrt{s} = 1.96$ TeV, collected with the CDF II detector at the Fermilab Tevatron. Exploiting the largest available charmed baryon sample, we measure masses and decay widths with uncertainties comparable to the world averages for Σ_c states, and significantly smaller uncertainties than the world averages for excited Λ_c^+ states.

I. INTRODUCTION

Hadrons containing a b or c quark are referred to as heavy-quark hadrons and provide an interesting laboratory for studying and testing quantum chromodynamics (QCD), the theory of strong interactions [1,2]. Because the strong coupling constant α_s is large for interactions involving small momentum transfer, masses and decay widths of the heavy-quark states cannot be calculated within the framework of perturbative QCD. As a result, many different approaches have been developed, for example, based on heavy-quark effective theory (HQET) [3], nonrelativistic and relativistic potential models [4], or lattice QCD [5].

In the limit of HQET, heavy-quark mesons, comprised of one heavy and one light quark, are the closest analogy to the hydrogen atom, which provided important tests of quantum electrodynamics. Heavy-quark baryons, comprised of one heavy and two light quarks, extend the hydrogen atom analogy of HQET by treating the two light quarks as a diquark system. This leads to degenerate spin-1/2 states resulting from the combination of a spin-0, or a spin-1, light diquark with the heavy quark, and thus represents a complementary situation compared to heavy-quark mesons. Measurements of the mass spectrum and spin splittings of heavy-quark baryons are important for validating the theoretical techniques, and build confidence in their predictions for other heavy flavor studies.

In this paper, we measure the properties of heavy-quark baryons that contain a c quark, namely, the resonances $\Lambda_c(2595)^+$, $\Lambda_c(2625)^+$, $\Sigma_c(2455)^{++,0}$, and $\Sigma_c(2520)^{++,0}$. For simplification, we refer to $\Sigma_c^{++,0}$ as Σ_c wherever this information is not crucial. Throughout the paper, the use of a specific particle state implies the use of the charge-conjugate state as well. The quark model predicts the $\Lambda_c(2595)^+$ and $\Lambda_c(2625)^+$, referred to as Λ_c^{*+}, to be the lowest orbital excitations of the Λ_c^+ ground state with a spin-0 light diquark. The two Σ_c resonances are expected to have no orbital excitation and a spin-1 light diquark.

Some theoretical predictions of the resonance masses are summarized in Table I, where Ref. [6] uses lattice QCD, Refs. [7–9] are based on the quark model, Ref. [10] employs QCD sum rules and Ref. [11] uses a

bag model. There are a few calculations that predict the $\Sigma_c(2455)$ natural width in the region of 1–3 MeV/c^2 [12–17] and the $\Sigma_c(2520)$ width to be about 18 MeV/c^2 [17]. No predictions are available for the $\Lambda_c(2595)^+$ and $\Lambda_c(2625)^+$ widths.

Experimental observation of all four states studied here and measurements of some of their properties have been reported earlier [18–25]. We list the world average masses and widths in Table II, omitting Σ_c^+ states, which are difficult to reconstruct with the CDF II detector due to the inefficiency in π^0 identification. For $\Sigma_c(2455)$, many measurements exist with most of the information coming from CLEO [18] and FOCUS [19]. Experimental information on the $\Sigma_c(2520)$ states comes exclusively from CLEO [20,21] and it is worth noting that the two measurements of the $\Sigma_c(2520)^{++}$ mass are inconsistent. For $\Lambda_c(2595)^+$ and $\Lambda_c(2625)^+$ three experiments have contributed, namely, ARGUS [22], E687 at Fermilab [23,24] and CLEO [25], all of which suffer from rather small data samples. In addition, Blechman and co-authors [27] showed that a

TABLE I. Theoretical predictions for the masses of the charmed baryons under study. All values are given in MeV/c^2.

Hadron	[6]	[7]	[8,9]	[10]	[11]
$\Sigma_c(2455)$	2452	2455	2439	2400 ± 310	2393
$\Sigma_c(2520)$	2538	2519	2518	2560 ± 240	2489
$\Lambda_c(2595)^+$	$\cdots$	2625	2598	2530 ± 220	$\cdots$
$\Lambda_c(2625)^+$	$\cdots$	2636	2628	2580 ± 240	$\cdots$

TABLE II. World average values of the mass differences between the charmed baryon resonances and the Λ_c^+ mass, ΔM, and their natural widths, Γ [26].

Hadron	ΔM [MeV/c^2]	Γ [MeV/c^2]
$\Sigma_c(2455)^{++}$	167.56 ± 0.11	2.23 ± 0.30
$\Sigma_c(2455)^0$	167.30 ± 0.11	2.2 ± 0.4
$\Sigma_c(2520)^{++}$	231.9 ± 0.6	14.9 ± 1.9
$\Sigma_c(2520)^0$	231.6 ± 0.5	16.1 ± 2.1
$\Lambda_c(2595)^+$	308.9 ± 0.6	$3.6^{+2.0}_{-1.3}$
$\Lambda_c(2625)^+$	341.7 ± 0.6	<1.9 at 90% C.L.

more sophisticated treatment of the mass line shape, which takes into account the proximity of the $\Lambda_c(2595)^+$ mass to the sum of the masses of its decay products, yields a $\Lambda_c(2595)^+$ mass which is 2–3 MeV/c^2 lower than the one observed. The $\Sigma_c(2455)$ and $\Sigma_c(2520)$ decay directly to $\Lambda_c^+ \pi$, whereas the $\Lambda_c(2595)^+$ and $\Lambda_c(2625)^+$ end mainly in a $\Lambda_c^+ \pi\pi$ final state with dominating decays through intermediate Σ_c resonances. Therefore, these four resonances contribute to each other's background, which requires a dedicated cross-feed background modeling in each case.

In this analysis, we exploit a large sample of $\Lambda_c^+ \rightarrow pK^-\pi^+$ decays produced in $p\bar{p}$ collisions at $\sqrt{s} = 1.96$ TeV and collected by the CDF II detector. Measurements of the masses and widths of the charmed baryons are performed through fits to the reconstructed mass distributions calculated from the momenta of the final state tracks. We take into account all expected cross-feeds and threshold effects.

The paper is organized as follows. In Sec. II we briefly describe the CDF II detector and the trigger components important for this analysis. Secs. III and IV describe the candidate reconstruction and selection, respectively. In Sec. V we explain the fits involved in the measurements, followed by a discussion of systematic uncertainties in Sec. VI. Finally the results and conclusions are presented in Sec. VII.

II. CDF II DETECTOR AND TRIGGER

Among the components and capabilities of the CDF II detector [28], the tracking system is the one most relevant to this analysis. It lies within a uniform, axial magnetic field of 1.4 T strength. The inner tracking volume up to a radius of 28 cm is comprised of 6–7 layers of double-sided silicon microstrip detectors [29]. An additional layer of single-sided silicon is mounted directly on the beam-pipe at a radius of 1.5 cm, allowing excellent resolution on the impact parameter d_0, defined as the distance of closest approach of the track to the interaction point in the plane transverse to the beam line. The silicon detector provides a vertex resolution of approximately 15 μm in the transverse and 70 μm in the longitudinal direction. The remainder of the tracking volume from a radius of 40 to 137 cm is occupied by an open-cell drift chamber (COT) [30], providing a transverse momentum resolution of $\sigma(p_T)/p_T^2 \approx 0.1\%/(\text{GeV}/c)$. Hadron identification, which is crucial for distinguishing slow kaons and protons from pions, is achieved by a likelihood combination of information from a time-of-flight system (TOF) [31] and ionization energy loss in the COT. This offers about 1.5σ separation between kaons, or protons, and pions.

A three-level trigger system is used for the online event selection. The most important device for this analysis at level 1 is the extremely fast tracker (XFT) [32]. It identifies charged particles using information from the COT and measures their transverse momenta and azimuthal angles around the beam direction. The basic requirement at level 1 is two charged particles with transverse momentum, p_T, greater than 2 GeV/c. At level 2, the silicon vertex trigger [33] adds silicon hit information to the XFT tracks, thus allowing the precise measurement of impact parameters of tracks. The two level 1 tracks are required to have impact parameters between 0.1 and 1 mm and to be consistent with coming from a common vertex displaced from the interaction point by at least 100 μm in the plane transverse to the beam line. The level 3 trigger is implemented in software and provides the final online selection by confirming the first two trigger-level decisions using a more precise reconstruction similar to the offline software. This trigger is designed to collect hadronic decays of long-lived particles such as b and c hadrons. As determined by a study of the impact parameter distributions, the sample of charmed baryons recorded by the trigger consists of approximately equal contributions from Λ_b decays and direct $c\bar{c}$ production.

III. DATA SET AND RECONSTRUCTION

The analysis is performed on a data set collected by the CDF II detector at the Tevatron $p\bar{p}$ collider between February 2002 and June 2009 corresponding to an integrated luminosity of 5.2 fb^{-1}. The data were accumulated using the displaced two track vertex trigger described in the previous Section.

The offline reconstruction of candidates starts with refitting tracks using pion, kaon and proton mass hypotheses to properly take into account differences in the multiple scattering and ionization energy loss. In the second step, three tracks, one with pion, one with kaon, and one with proton mass hypotheses, are combined to form a Λ_c^+ candidate. The three tracks are subjected to a kinematic fit that constrains them to originate from a common vertex. We require that the proton and pion candidates have the same charge and that the total charge of all three tracks is ± 1. To construct $\Sigma_c(2455)$ and $\Sigma_c(2520)$ candidates we combine each Λ_c^+ candidate with one of the remaining tracks in the event using a pion mass hypothesis. The $\Lambda_c(2595)^+$ and $\Lambda_c(2625)^+$ candidates are obtained by combining each Λ_c^+ candidate with all possible oppositely charged track pairs taken from the remaining tracks in the event using the pion mass hypothesis for each of them. The tracks forming each baryon candidate are subjected to a kinematic fit that constrains them to originate from a common point. In each step of the reconstruction, standard quality requirements on tracks and vertices are used to ensure well-measured masses and decay-positions.

We use simulated events to estimate the detector mass resolutions of the charmed baryons studied here. The decays are simulated by means of the EVTGEN package [34], where the Λ_c^+ is forced to decay into $pK^-\pi^+$ with its resonance structure taken into account. Afterwards, the

generated events are passed through the detector simulation and then reconstructed by the same software used for data.

IV. CANDIDATE SELECTION

The selection of the candidates is done in two steps. In each one we first impose some quality requirements to suppress the most obvious background. For the surviving candidates we use a neural network to distinguish signal from background. Since all final states feature a Λ_c^+ daughter, the first step is the Λ_c^+ selection. In the second step, we perform a dedicated selection of the four states under study. All neural networks are constructed with the NEUROBAYES package [35,36] and trained, only using data, by means of the $_sPlot$ technique [37,38]. This technique assigns a weight to each candidate proportional to the probability that the candidate is signal. The candidate weight is based on the discriminating variables, which are required to be independent of the ones used in the neural network training. In our case, the discriminating variable is the invariant mass of the candidate. In the training, each candidate enters with a weight calculated from the signal probability that is derived from its mass. Based on these weights, the neural network can learn the features of signal and background events. Since we use only data for the neural network trainings, we randomly split each sample into two parts (even and odd event numbers) and train two networks. Each of them is then applied to the complementary subsample in order to maintain a selection which is trained on a sample independent from the one to which it is applied. This approach avoids a bias of the selection originating from statistical fluctuations possibly learnt by the network. Additionally, using candidates from two different mass regions populated by background only for the training, we verify that the network selection does not depend on the mass or create an artificial excess in the spectrum.

A. Λ_c^+ selection

The $\Lambda_c^+ \to pK^-\pi^+$ candidates are required to decay to a proton with $p_T > 1.9$ GeV/c and other particles with $p_T > 400$ MeV/c. The displacement of the associated secondary vertex, projected onto the Λ_c^+ transverse momentum direction, to the beam, L_{xy}, is required to be greater than 0.25 mm. In addition, we use particle identification information from the TOF and dE/dx from the COT. We combine the two sources of information for each track t into a single variable

$$LL_i(t) = \frac{P_{dE/dx}^i(t) P_{\mathrm{TOF}}^i(t)}{\sum\limits_{j=\pi,K,p} f_j P_{dE/dx}^j(t) P_{\mathrm{TOF}}^j(t)}, \qquad (1)$$

where the index i denotes the hypothesis of the particle type. The $P_{\mathrm{TOF}}^i(t)$ is the probability to observe the measured time-of-flight given a particle of type i, and $P_{dE/dx}^i(t)$
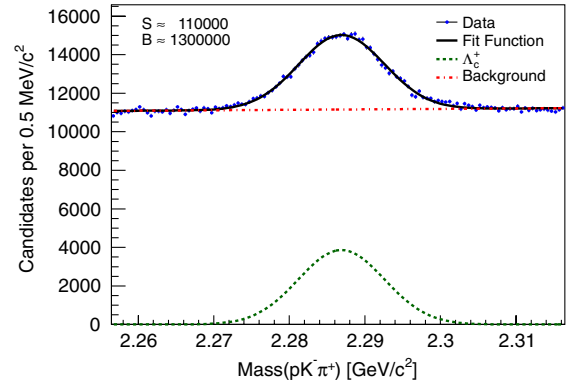

FIG. 1 (color online). The mass distribution of Λ_c^+ candidates used to train one of the two neural networks for the Λ_c^+ selection.

is the probability to observe the measured dE/dx. The fractions f_j are $f_\pi = 0.7$, $f_K = 0.2$, and $f_p = 0.1$, as estimated from TOF information of a generic background sample. We apply the requirement $LL_p > 0.6$ on the proton track and $LL_K > 0.2$ on the kaon track. In case TOF or dE/dx information is not available for a given track, we do not impose the corresponding requirement. The mass distribution of the candidates with even event numbers is shown in Fig. 1. A fit with a Gaussian signal and a linear background function defines the probability density functions (PDFs) used to calculate the $_sPlot$ weights for the Λ_c^+ network training. The corresponding distribution of odd-numbered events is similar.

The full list of input quantities of the neural network, sorted by their importance, can be found in Table III. In the table, d_0 denotes the impact parameter with respect to the primary vertex of the $p\bar{p}$ interaction for a track in the plane transverse to the beam direction, σ_{d_0} its uncertainty, $\chi^2(\Lambda_c^+)$ the quality of the kinematic fit of the Λ_c^+ candidate, and $\cos(\sphericalangle(\Lambda_c^+, t))$ the cosine of the angle between the momentum of the Λ_c^+ candidate in the lab frame and the momentum of the proton or kaon track in the Λ_c^+ rest frame. These angles carry information about the resonant substructure of the decay $\Lambda_c^+ \to pK^-\pi^+$.

To demonstrate the ability of the neural network to classify signal and background, the mass distributions of Λ_c^+ candidates with even event numbers before and after

TABLE III. Inputs to the neural network for the Λ_c^+ selection sorted by their importance.

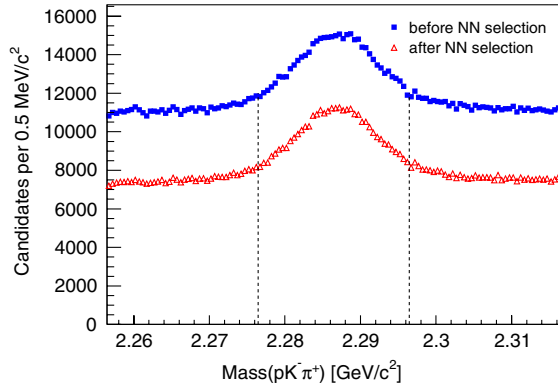| Index	Variable	Index	Variable
1	$LL_p(p)$	8	$p_T(p)$
2	$\sigma_{L_{xy}}(\Lambda_c^+)$	9	$\cos(\sphericalangle(\Lambda_c^+, K))$
3	$LL_K(K)$	10	$p_T(\pi)$
4	$\cos(\sphericalangle(\Lambda_c^+, p))$	11	$d_0/\sigma_{d_0}(K)$
5	$\chi^2(\Lambda_c^+)$	12	$p_T(K)$
6	$L_{xy}(\Lambda_c^+)$	13	$d_0/\sigma_{d_0}(p)$
7	$d_0/\sigma_{d_0}(\pi)$		

FIG. 2 (color online). The mass distributions of Λ_c^+ candidates before (blue full squares) and after (red open triangles) requiring their neural network output to correspond to an *a posteriori* signal probability greater than 2.5%. The vertical dashed lines indicate a ± 10 MeV/c^2 region around the nominal Λ_c^+ mass [26] used for the selection of the Σ_c and Λ_c^{*+} states.

requiring their neural network output to correspond to an *a posteriori* signal probability greater than 2.5% is shown in Fig. 2. This requirement leads to a background reduction of 32% while keeping 97% of the signal. We use the output of the Λ_c^+ neural network as input to the neural networks for selecting the Σ_c and Λ_c^{*+} resonances.

B. $\Sigma_c(2455)$ and $\Sigma_c(2520)$ selection

The $\Sigma_c(2455)^{++,0}$ and $\Sigma_c(2520)^{++,0} \rightarrow \Lambda_c^+ \pi^{+,-}$ selection starts with the application of a few loose requirements to remove the most obvious background, followed by the use of a neural network. We require the *a posteriori* signal probability of the Λ_c^+ neural network to be greater than 2.5% (see Fig. 2), the $p_T(\pi)$ of the added pion to be greater than 400 MeV/c, $d_0(\pi) < 1.5$ mm, and the mass of the Λ_c^+ candidate to be within ± 10 MeV/c^2 of the nominal Λ_c^+ mass [26], $2276.46 < M(pK^-\pi^+) < 2296.46$ MeV/c^2 (see Fig. 2). These requirements are common for both neutral and doubly-charged states. The mass difference $\Delta M = M(\Sigma_c) - M(\Lambda_c^+)$ distributions of all the $\Lambda_c^+\pi^+$

and $\Lambda_c^+\pi^-$ candidates are shown in Fig. 3. In the ΔM definition, $M(\Sigma_c)$ and $M(\Lambda_c^+)$ correspond to the reconstructed masses of the Σ_c and Λ_c^+ candidates.

The neural network for the final selection of the $\Sigma_c(2455)$ and $\Sigma_c(2520)$ candidates uses five input quantities. Ordered by their importance, these are the output of the Λ_c^+ neural network $NN(\Lambda_c^+)$, the proper decay time of the Σ_c candidate $t(\Sigma_c) = (L_{xy}(\Sigma_c) \cdot M(\Sigma_c))/(c \cdot p_T(\Sigma_c))$, the quality of the kinematic fit of the Σ_c candidate $\chi^2(\Sigma_c)$, the uncertainty of the Σ_c impact parameter in the transverse plane $\sigma_{d_0}(\Sigma_c)$, and the impact parameter in the transverse plane of the pion from the Σ_c decay $d_0(\pi)$. Independent neural networks are employed for Σ_c^{++} and Σ_c^0. The training itself is performed using candidates in the mass difference region from 155 to 180 MeV/c^2. Although this includes only $\Sigma_c(2455)$ candidates, it is applied to select $\Sigma_c(2520)$ candidates as well. The $_sPlot$ weights are determined by a fit to the ΔM distribution with a Gaussian function for the signal and a linear function for the background PDF. We choose the threshold on the output of the Σ_c neural network to maximize $S/\sqrt{S+B}$, where S is the number of signal Σ_c events and B is the number of background events in ΔM between 162.3 and 172.3 MeV/c^2. The S and B yields are derived from a fit to the ΔM distribution which uses a Gaussian function for the signal and a linear function for the background and covers the ΔM range used for the neural network training. The resulting neural network output requirement is the same for both charge combinations and corresponds to an *a posteriori* signal probability of the neural networks greater than 10%. The ΔM distributions of the selected candidates are shown in Fig. 3.

C. $\Lambda_c(2595)^+$ and $\Lambda_c(2625)^+$ selection

The initial step of the $\Lambda_c(2595)^+$ and $\Lambda_c(2625)^+ \rightarrow \Lambda_c^+\pi^+\pi^-$ selection requires the *a posteriori* signal probability of the Λ_c^+ neural network to be greater than 2.5%, $2276.46 < M(pK^-\pi^+) < 2296.46$ MeV/c^2 (see Fig. 2), $p_T(\pi)$ of both added pions to be greater than
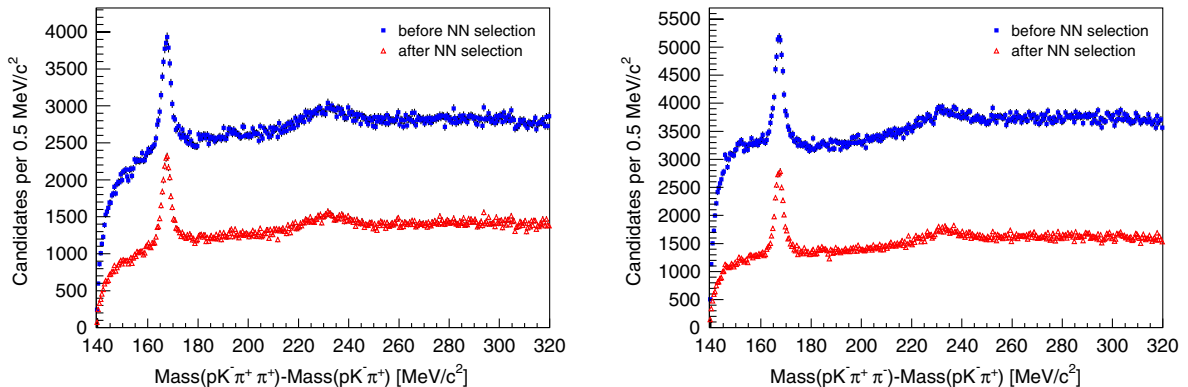

FIG. 3 (color online). The mass difference distributions of the $\Lambda_c^+\pi^+$ (left) and $\Lambda_c^+\pi^-$ (right) candidates before (blue full squares) and after (red open triangles) applying the neural network selection.
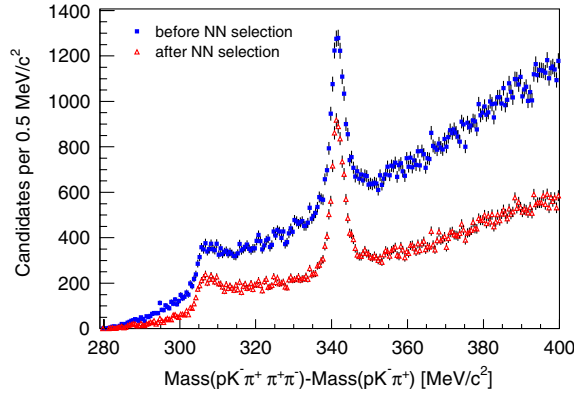
FIG. 4 (color online). The mass difference distribution of the $\Lambda_c^+ \pi^+ \pi^-$ candidates before (blue full squares) and after (red open triangles) applying the neural network selection.

400 MeV/c, and the impact parameter of the object constructed from the two additional pions to be $d_0(\pi^+\pi^-) < 1.0$ mm. The mass difference $\Delta M = M(\Lambda_c^{*+}) - M(\Lambda_c^+)$ distribution is shown in Fig. 4.

We use the ΔM region between 327 and 357 MeV/$c^2$for the neural network training. Although this includes only $\Lambda_c(2625)^+$ candidates, it is applied to select $\Lambda_c(2595)^+$ candidates as well. The $_s\mathcal{P}lot$ weights are based on a fit to the ΔM distribution with a Gaussian function for the signal and a linear function for the background PDF. The neural network uses four inputs. Ordered by their importance, these are the quality of the Λ_c^{*+} kinematic fit $\chi^2(\Lambda_c^{*+})$, the uncertainty of the impact parameter of the combined two-pion object $\sigma_{d_0}(\pi^+\pi^-)$, the output of the Λ_c^+ neural network $NN(\Lambda_c^+)$, and the proper decay time of the Λ_c^{*+} candidate $t(\Lambda_c^{*+})$. We choose the requirement that maximizes $S/\sqrt{S+B}$, corresponding to an *a posteriori* signal probability of the neural network greater than 12.5%. The S and B yields are derived from a fit to the ΔM distribution using a Gaussian function for the signal and a linear function for the background, where we consider events in the region $336.7 < \Delta M < 346.7$ MeV/c^2. The resulting mass difference distribution after the final requirements is shown in Fig. 4.

V. FIT DESCRIPTION

To determine the mass differences relative to the Λ_c^+ and the widths of the six studied states, we perform binned maximum likelihood fits to three separate mass difference distributions. The first two are $\Lambda_c^+\pi^+$ and $\Lambda_c^+\pi^-$, where the states $\Sigma_c(2455)^{++,0}$ and $\Sigma_c(2520)^{++,0}$ are studied. The last one is $\Lambda_c^+\pi^+\pi^-$ for $\Lambda_c(2595)^+$ and $\Lambda_c(2625)^+$. In the case of the Σ_c states, part of the background comes from Λ_c^{*+} decays and thus has different properties compared to the combinatorial background. On the other hand, when fitting Λ_c^{*+} states, there is a background contribution from random $\Sigma_c^{++,0}\pi^{-,+}$ combinations which have a threshold close to the $\Lambda_c(2595)^+$ state.

The negative logarithm of the likelihood function has a general form of

$$-\ln\mathcal{L}(\vec{a}) = -\sum_{j=1}^{J} \ln\left(\frac{\mu_j^{n_j} e^{-\mu_j}}{n_j!}\right)$$

$$= -\sum_{j=1}^{J} n_j \ln\mu_j + \sum_{j=1}^{J} \mu_j + \sum_{j=1}^{J} \ln(n_j!), \quad (2)$$

where $\vec{a}$ are the free parameters, J is the number of bins in the histogram of the corresponding mass difference distribution, n_j is the number of entries in bin j, and μ_j is the expected number of entries in bin j. The values μ_j are obtained using the function

$$\mu(\Delta M) = N_1 \cdot s_1(\Delta M) + N_2 \cdot s_2(\Delta M) + b(\Delta M), \quad (3)$$

where $s_1(\Delta M)$ and $s_2(\Delta M)$ are the PDFs for the two signals, $b(\Delta M)$ is the background function and N_i are the corresponding numbers of events. All three PDFs depend on a subset of the free parameters $\vec{a}$. The function is evaluated at the bin center to calculate the expectation for μ_j. While the general structure is the same in all three fits, the PDFs are specific to Σ_c and Λ_c^{*+} states.

A. $\Sigma_c(2455)$ and $\Sigma_c(2520)$ fit

In each of the two distributions we need to parametrize two signals and several background components. We use a 150–320 MeV/c^2range to avoid complications arising from the description of the steep rise of the background at threshold. Both $\Sigma_c(2455)$ and $\Sigma_c(2520)$ are described by a nonrelativistic Breit-Wigner function,

$$\frac{dN}{d\Delta M} \propto \frac{\Gamma}{(\Delta M - \Delta M_0)^2 + \Gamma^2/4}, \quad (4)$$

convolved with a resolution function. The resolution function itself is parametrized by three Gaussians with mean zero and the other parameters derived from simulated events. The average width of the resolution function is about 1.6 MeV/$c^2$for $\Sigma_c(2455)^{++,0}$ and about 2.6 MeV/$c^2$for $\Sigma_c(2520)^{++,0}$. For illustration, the simulated $\Sigma_c(2520)^0$ mass resolution is shown in Fig. 5.

We introduce a single common scaling factor s for the widths of all three Gaussians to correct for a possible mismatch in our mass resolution estimate. This scaling factor is allowed to float within a Gaussian constraint in the fit, what corresponds to adding

$$0.5 \cdot \left(\frac{s - \mu}{\sigma}\right)^2 \quad (5)$$

with $\mu = 1$ and $\sigma = 0.2$, reflecting a 20% uncertainty on the mass resolution (see Sec. VI), to the negative logarithm of the likelihood.

Three different types of background are considered, namely, random combinations without real Λ_c^+, combinations of real Λ_c^+ with a random pion, and events due to the decay of Λ_c^{*+} to $\Lambda_c^+\pi^+\pi^-$. The random combinations
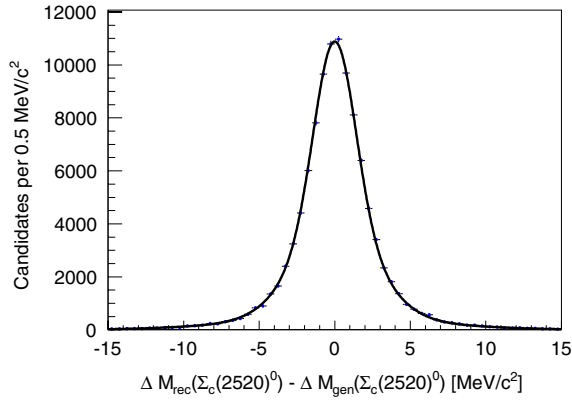
FIG. 5 (color online). $\Sigma_c(2520)^0$ mass resolution obtained from simulated events by subtracting the generated mass difference $\Delta M_{\text{gen}}(\Sigma_c(2520)^0)$ from the reconstructed one $\Delta M_{\text{rec}}(\Sigma_c(2520)^0)$. The fitted function is a combination of three Gaussians with mean zero.

without a real Λ_c^+ dominate and are described by a second-order polynomial with shape and normalization derived in a fit to the ΔM distribution from the Λ_c^+ mass sidebands $2261.46 < M(pK^-\pi^+) < 2266.46 \text{ MeV}/c^2$ and $2306.46 < M(pK^-\pi^+) < 2311.46 \text{ MeV}/c^2$. In the Σ_c fit, this contribution is allowed to float within a Gaussian constraint implemented by the addition of

$$0.5 \cdot \vec{\Delta}^T \cdot \mathbf{V}^{-1} \cdot \vec{\Delta} \tag{6}$$

to the negative logarithm of the likelihood, where $\mathbf{V}$ is the covariance matrix of the fit to the ΔM distribution from the Λ_c^+ mass sidebands and $\vec{\Delta}$ is the vector of parameters of the second-order polynomial. The fits to the distributions from the Λ_c^+ mass sidebands can be found in Fig. 6. The difference between doubly-charged and neutral spectra is due to $D^*(2010)^+ \to D^0\pi^+$ mesons with multibody D^0 decays, where not all D^0 decay products are reconstructed. In order to describe this reflection, an additional Gaussian function is used. The second background source consisting of real Λ_c^+ combined with a random pion is modeled by a third-order polynomial, where all parameters are left free
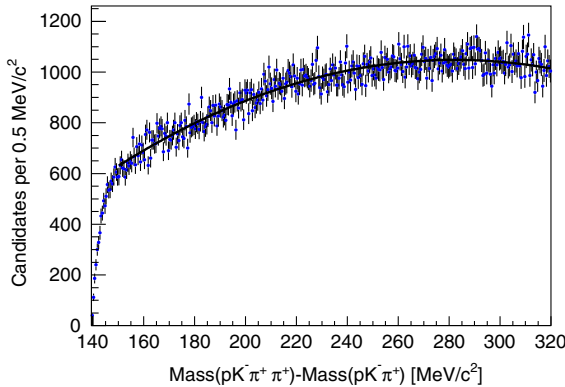
in the fit. The background originating from Λ_c^{*+} decays is described using theoretical considerations. With good approximation, there are two states that contribute, namely $\Lambda_c(2595)^+$ and $\Lambda_c(2625)^+$, decaying into a $\Lambda_c^+\pi^+\pi^-$ final state. The $\Lambda_c(2595)^+$ decays dominantly to a $\Sigma_c\pi$ final state [26] and thus contributes mainly to the signal. We therefore neglect its contributions to the backgrounds in the $\Lambda_c\pi$ distributions. On the other hand, the $\Lambda_c(2625)^+$ decay is dominantly nonresonant [26]. To model it, we start from a flat $\Lambda_c^+\pi^+\pi^-$ Dalitz plot and project it on the appropriate axis. Since the shape of the projection depends on the reconstructed $\Lambda_c(2625)^+ \to \Lambda_c^+\pi^+\pi^-$ mass, we use ten different values of this mass and weight their contribution according to the $\Lambda_c(2625)^+$ shape we obtain from our fit to the $\Lambda_c^+\pi^+\pi^-$ data. This contribution amounts to about 2% of the total background.

The full fit to the ΔM distribution, containing all signal and background components, can be found in Fig. 7. The χ^2 value of the Σ_c^{++} fit is 340 (324 degrees of freedom) and that of the Σ_c^0 fit is 384 (321 degrees of freedom).

B. $\Lambda_c(2595)^+$ and $\Lambda_c(2625)^+$ fit

The fit for $\Lambda_c(2595)^+$ and $\Lambda_c(2625)^+$ includes two signals and several background components and is performed in a ΔM region from 290 to 400 MeV/c^2. Previous measurements of the $\Lambda_c(2595)^+$ properties indicate that it decays dominantly to the final state $\Sigma_c\pi$, with the threshold very close to the $\Lambda_c(2595)^+$ mass [26]. This introduces an additional complication to the fit compared to the Σ_c case. Blechman *et al.* [27] showed that taking into account the mass dependence of the natural width yields a lower $\Lambda_c(2595)^+$ mass measurement than observed by previous experiments. With the present event sample we are more sensitive to the details of the $\Lambda_c(2595)^+$ line shape than previous analyses and include this dependence in the model.

The $\Lambda_c(2595)^+$ parametrization follows Ref. [27]. The state is described by a nonrelativistic Breit-Wigner function of the form
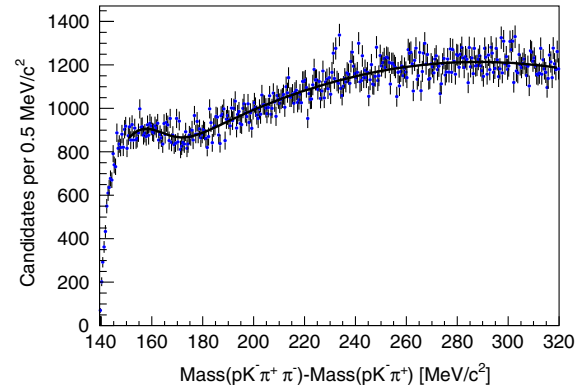

FIG. 6 (color online).   Fit to the $M(pK^-\pi^+\pi^+) - M(pK^-\pi^+)$ (left) and $M(pK^-\pi^+\pi^-) - M(pK^-\pi^+)$ (right) distributions of the candidates from Λ_c^+ mass sidebands.
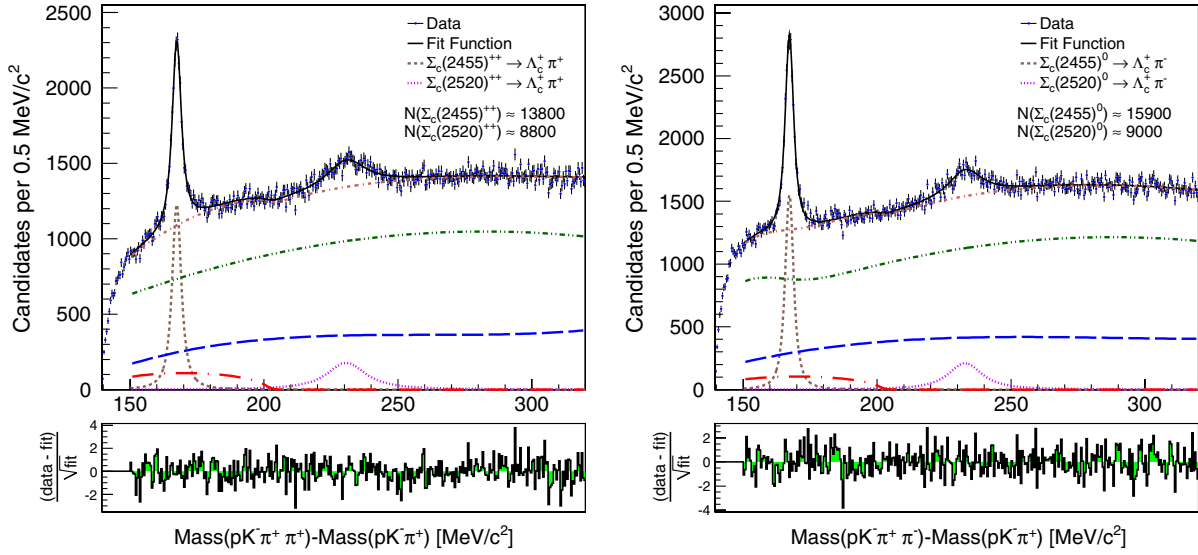
FIG. 7 (color online).   The $M(pK^-\pi^+\pi^+) - M(pK^-\pi^+)$ (left) and $M(pK^-\pi^+\pi^-) - M(pK^-\pi^+)$ (right) distributions obtained from data (points with error bars) together with the fits (black solid line). The brown dashed and purple dotted lines correspond to the two signal contributions, the green dash-double-dotted line represents the combinatorial background without real Λ_c^+, the blue long-dashed line shows real Λ_c^+ combined with a random pion and the red long-dash-dotted line represents a reflection from Λ_c^{*+} decays. The red dash-dotted line corresponds to the sum of all three background contributions.

$$\frac{dN}{d\Delta M} \propto \frac{\Gamma(\Lambda_c^+\pi^+\pi^-)}{(\Delta M - \Delta M_{\Lambda_c(2595)^+})^2 + (\Gamma(\Lambda_c^+\pi^+\pi^-) + \Gamma(\Lambda_c^+\pi^0\pi^0))^2/4}, \tag{7}$$

where $\Gamma(\Lambda_c^+\pi^+\pi^-)$ and $\Gamma(\Lambda_c^+\pi^0\pi^0)$ are the mass-dependent partial widths to the $\Lambda_c^+\pi^+\pi^-$ and $\Lambda_c^+\pi^0\pi^0$ final states. Assuming that those two final states saturate nearly 100% of the $\Lambda_c(2595)^+$ decay width, the sum in the denominator corresponds to the total width. The two partial widths are derived in Ref. [39] as

$$\Gamma(\Lambda_c^+\pi^+\pi^-) = \frac{g_2^2}{16\pi^3 f_\pi^4} m_{\Lambda_c^+}$$
$$\times \int dE_1 dE_2 (|\vec{p}_2|^2 |A(E_1)|^2 + |\vec{p}_1|^2 |B(E_2)|^2$$
$$+ 2\vec{p}_1 \cdot \vec{p}_2 \mathrm{Re}[A(E_1)B^*(E_2)]), \tag{8}$$

$$\Gamma(\Lambda_c^+\pi^0\pi^0) = \frac{g_2^2}{16\pi^3 f_\pi^4} m_{\Lambda_c^+}$$
$$\times \int dE_1 dE_2 (|\vec{p}_2|^2 |C(E_1)|^2 + |\vec{p}_1|^2 |C(E_2)|^2$$
$$+ 2\vec{p}_1 \cdot \vec{p}_2 \mathrm{Re}[C(E_1)C^*(E_2)]). \tag{9}$$

Here, $f_\pi = 132$ MeV/c^2 is the pion decay constant [40], $m_{\Lambda_c^+}$ is the world average Λ_c^+ mass, E_1, E_2 are the energies of the two pions in the rest frame of the $\Lambda_c(2595)^+$, and $\vec{p}_1$, $\vec{p}_2$ are the corresponding momenta. Following Ref. [27], the coupling constant g_2 is determined by the Σ_c decay width using the relation

$$\Gamma_{\Sigma_c} = \frac{g_2^2}{2\pi f_\pi^2} \frac{m_{\Lambda_c^+}}{m_{\Sigma_c}} |\vec{p}_\pi|^3, \tag{10}$$

with m_{Σ_c} being the world average mass of the $\Sigma_c(2455)$ and $\vec{p}_\pi$ the momentum of the pion from the $\Sigma_c(2455)$ decay to $\Lambda_c\pi$ in the $\Sigma_c(2455)$ rest frame. From the world average $\Gamma_{\Sigma_c} = 2.2$ MeV/c^2 [26] we obtain the value $g_2^2 = 0.365$ which is fixed in the fit. The amplitudes A, B, and C for the decays $\Lambda_c(2595)^+ \to \Sigma_c(2455)^0\pi^+$, $\Lambda_c(2595)^+ \to \Sigma_c(2455)^{++}\pi^-$, and $\Lambda_c(2595)^+ \to \Sigma_c(2455)^+\pi^0$ are parametrized as

$$A(E) = \frac{h_2 E}{\Delta m - \Delta m_{\Sigma_c^0} - E + i\Gamma_{\Sigma_c^0}/2}, \tag{11}$$

$$B(E) = \frac{h_2 E}{\Delta m - \Delta m_{\Sigma_c^{++}} - E + i\Gamma_{\Sigma_c^{++}}/2}, \tag{12}$$

$$C(E) = \frac{1}{2} \cdot \frac{h_2 E}{\Delta m - \Delta m_{\Sigma_c^+} - E + i\Gamma_{\Sigma_c^+}/2}. \tag{13}$$

In these definitions, $m_{\Sigma_c^{++,+,0}}$ and $\Gamma_{\Sigma_c^{++,+,0}}$ are the mass and the width of the $\Sigma_c(2455)^{++,+,0}$ taken from Ref. [26]. The coupling constant h_2, defined in Ref. [16], is related to the decay width of the $\Lambda_c(2595)^+$ and represents the actual quantity we measure instead of the natural width. This approach describes a purely S-wave decay, a possible
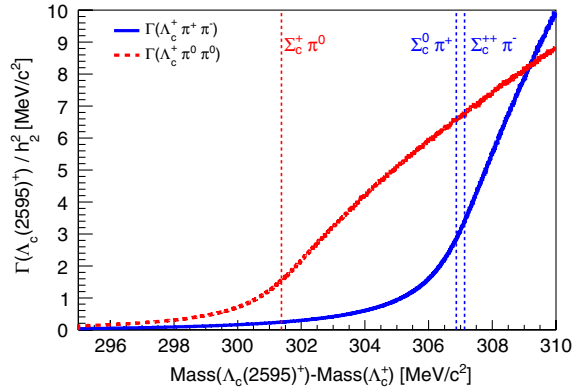
FIG. 8 (color online). Calculated dependence of $\Gamma(\Lambda_c^+ \pi^+ \pi^-)$ and $\Gamma(\Lambda_c^+ \pi^0 \pi^0)$ on $M(\Lambda_c(2595)^+) - M(\Lambda_c^+)$. The constant factor h_2^2 is determined by a fit to the experimental data.

FIG. 9 (color online). Fit to the $M(pK^- \pi^+ \pi^+ \pi^-) - M(pK^- \pi^+)$ distribution of the candidates from Λ_c^+ mass sidebands.

D-wave contribution is assumed to be negligible and ignored. For illustration, we show the dependence of the two partial widths on $M(\Lambda_c(2595)^+) - M(\Lambda_c^+)$ in Fig. 8. The shape defined by Eq. (7) is then numerically convolved with a resolution function determined from simulation and consisting of three Gaussians with mean zero. The average width of the resolution function is about 1.8 MeV/c^2. As for the Σ_c case, we introduce a common, Gaussian constrained, scaling factor for the widths of all three Gaussians, in order to account for the uncertainty in the width of the resolution function.

The signal PDF for the $\Lambda_c(2625)^+$ is the nonrelativistic Breit-Wigner function of Eq. (4) convolved with a three Gaussian resolution function determined from simulation, which has an average width of about 2.4 MeV/c^2. Again, all three Gaussians have mean zero and a common, Gaussian constrained, scaling factor for their widths is introduced.

The background consists of three different sources, which include combinatorial background without real Λ_c^+, real Λ_c^+ combined with two random pions, and real $\Sigma_c^{++,0}$ combined with a random pion. The combinator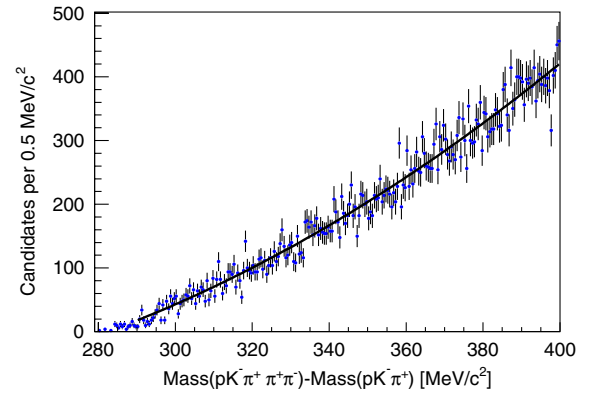ial background without real Λ_c^+ is parametrized by a second-order polynomial whose parameters are determined in a fit to the ΔM distribution of candidates from the Λ_c^+ mass sidebands, $2261.46 < M(pK^- \pi^+) < 2266.46$ MeV/c^2 and $2306.46 < M(pK^- \pi^+) < 2311.46$ MeV/c^2. This distribution is shown in Fig. 9 together with the fit. In the final fit, we keep the parameters for this background floating within a Gaussian constraint of the form of Eq. (6) to the values found in the fit to the candidates from the Λ_c^+ mass sidebands. The second source, consisting of real Λ_c^+ combined with two random pions, is parametrized by a second-order polynomial with all parameters allowed to float in the fit. The final source of background are real Σ_c combined with a random pion. For this source, the main issue is to have the proper shape close to the threshold. Small imperfections at higher ΔM can be ignored, as the second background source has enough flexibility to absorb it. The PDF of this Σ_c background is based on a constant function defined from the threshold to the end of the fit range. In order to take into account the natural widths as well as resolution effects, we use the weighted sum of ten such functions for both $\Sigma_c(2455)^{++}$ and $\Sigma_c(2455)^0$. Their thresholds and weights are chosen according to the shapes derived in the Σ_c fits shown in
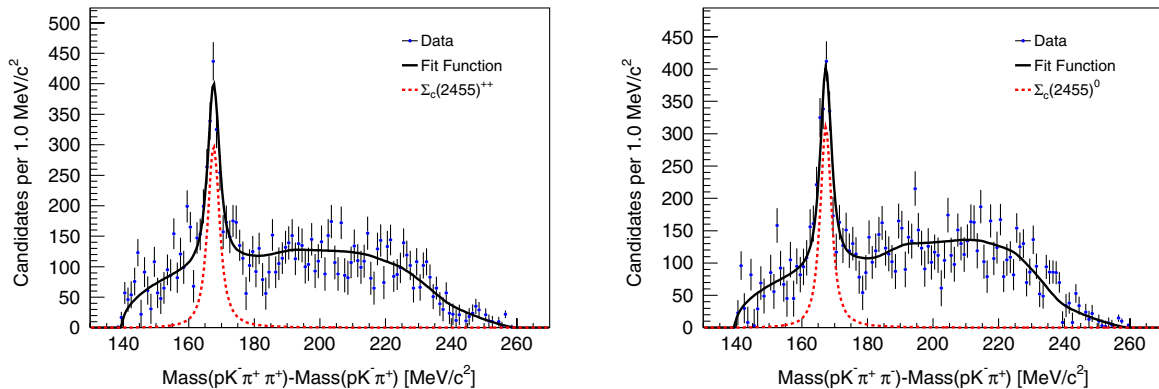

FIG. 10 (color online). Distributions of $M(\Sigma_c^{++}) - M(pK^- \pi^+)$ (left) and $M(\Sigma_c^0) - M(pK^- \pi^+)$ (right) for candidates with $M(\Lambda_c^{*+}) - M(pK^- \pi^+) > 355$ MeV/c^2 together with the fits.
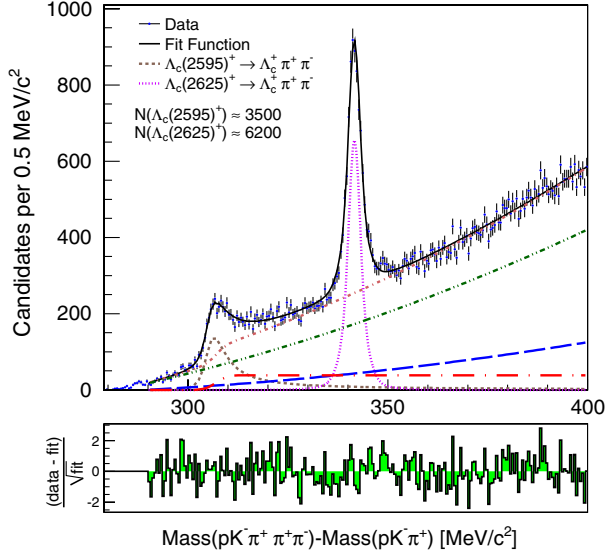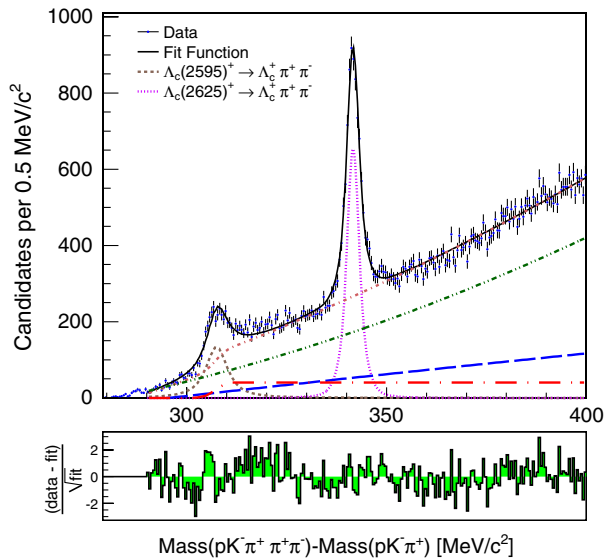
FIG. 11 (color online). The $M(pK^-\pi^+\pi^+\pi^-) - M(pK^-\pi^+)$ distribution obtained from data (points with error bars) together with the fit (black solid line). The brown dashed and purple dotted lines correspond to the two signal contributions, the green dash-double-dotted line represents the combinatorial background without real Λ_c^+, the blue long-dashed line shows real Λ_c^+ combined with two random pions and the red long-dash-dotted line represents real Σ_c combined with a random pion. The red dash-dotted line corresponds to the sum of all three background contributions.

FIG. 12 (color online). The $M(pK^-\pi^+\pi^+\pi^-) - M(pK^-\pi^+)$ distribution obtained from data (points with error bars) together with the fit (black solid line), where a Breit-Wigner function with a mass-independent decay width is used to model the $\Lambda_c(2595)^+$ line shape. Explanations of the various background contributions can be found in the caption of Fig. 11.

Fig. 7. The size of this contribution is constrained to the $\Sigma_c(2455)$ yield obtained from the fits to the $M(\Sigma_c) - M(pK^-\pi^+)$ distributions for candidates with $M(\Lambda_c^{*+}) - M(pK^-\pi^+) > 355$ MeV/c^2. These two distributions together with the fits are shown in Fig. 10.

The full fit to the ΔM distribution, containing all signal and background components, can be found in Fig. 11. The χ^2 value of the fit is 227 (206 degrees of freedom). Compared to that, the χ^2 value of a fit with a mass-independent $\Lambda_c(2595)^+$ decay width, shown in Fig. 12, increases to 286 (206 degrees of freedom).

VI. SYSTEMATIC UNCERTAINTIES

We investigate several systematic effects that can affect the measurements. Generally, they can be categorized as imperfect modeling by the simulation, imperfect knowledge of the momentum scale of the detector, ambiguities in the fit model, and uncertainties on the external inputs to the fit. In this Section we discuss how they can affect our results and the way we assess them. A summary of the assigned uncertainties can be found in Tables IV, V, and VI. To obtain the total systematic uncertainties, we add up the contributions from all sources in quadrature.

A. Mass resolution model

To properly describe the signal shapes, we need to understand the intrinsic mass resolution of the detector. Since we estimate this using simulated events, it is necessary to verify that the resolution obtained from simulation agrees with that in real data. We use $D^*(2010)^+ \to D^0\pi^+$ with $D^0 \to K^-\pi^+$ decays and $\psi(2S) \to J/\psi\pi^+\pi^-$ with $J/\psi \to \mu^+\mu^-$ decays for this purpose. We compare the resolution in data and simulated events as a function of the p_T of the pions added to D^0 or J/ψ as well as the instantaneous luminosity. We also compare the overall resolution scale between data and simulated events and find that all discrepancies are less than 20%, which we assign as uncertainty on our knowledge of the resolution function. The contribution from this uncertainty is already included in the uncertainties on the resonance parameters determined by the default fit with Gaussian constraint on the resolution scaling factor s, the resulting values for which are listed in Table VII. These values are consistent with 1, indicating that the resolution is well understood within the assigned uncertainty. To disentangle it from the statistical component, we repeat the fits on data without multiplying the widths of the resolution function by the scaling factor s from Eq. (5). The systematic uncertainty due to the imperfect modeling of the resolution function is then obtained by the difference in quadrature of the uncertainty of the fit with and without the Gaussian constraint. This uncertainty in the resolution has a large impact on the natural widths, but a negligible effect on the mass differences.

TABLE IV. Systematic uncertainties on the measurements of the mass differences and decay widths of the Σ_c^{++} resonances. The corresponding statistical uncertainties are listed for comparison.

Source	$\Delta M(\Sigma_c(2455)^{++})$ [MeV/c^2]	$\Gamma(\Sigma_c(2455)^{++})$ [MeV/c^2]	$\Delta M(\Sigma_c(2520)^{++})$ [MeV/c^2]	$\Gamma(\Sigma_c(2520)^{++})$ [MeV/c^2]
Resolution model	$\cdots$	0.40	$\cdots$	0.69
Momentum scale	0.12	0.20	0.12	0.20
Fit model	0.02	$\cdots$	0.11	1.16
External inputs	$\cdots$	$\cdots$	$\cdots$	$\cdots$
Sum	0.12	0.45	0.16	1.36
Statistical	0.04	0.13	0.56	2.12

TABLE V. Systematic uncertainties on the measurements of the mass differences and decay widths of the Σ_c^0 resonances. The corresponding statistical uncertainties are listed for comparison.

Source	$\Delta M(\Sigma_c(2455)^0)$ [MeV/c^2]	$\Gamma(\Sigma_c(2455)^0)$ [MeV/c^2]	$\Delta M(\Sigma_c(2520)^0)$ [MeV/c^2]	$\Gamma(\Sigma_c(2520)^0)$ [MeV/c^2]
Resolution model	$\cdots$	0.45	$\cdots$	0.70
Momentum scale	0.12	0.20	0.12	0.20
Fit model	0.02	$\cdots$	0.11	1.16
External inputs	$\cdots$	$\cdots$	$\cdots$	$\cdots$
Sum	0.12	0.49	0.16	1.37
Statistical	0.03	0.11	0.43	1.82

TABLE VI. Systematic uncertainties on the measurements of the mass differences of the Λ_c^{*+} resonances and the pion coupling constant h_2^2 ($\Gamma(\Lambda_c(2595)^+)$). The corresponding statistical uncertainties are listed for comparison.

Source	$\Delta M(\Lambda_c(2595)^+)$ [MeV/c^2]	h_2^2	$\Gamma(\Lambda_c(2595)^+)$ [MeV/c^2]	$\Delta M(\Lambda_c(2625)^+)$ [MeV/c^2]
Resolution model	0.06	0.03	0.22	$\cdots$
Momentum scale	0.12	0.03	0.20	0.12
Fit model	$\cdots$	$\cdots$	$\cdots$	$\cdots$
External inputs	0.15	0.06	0.36	$\cdots$
Sum	0.20	0.07	0.47	0.12
Statistical	0.14	0.04	0.30	0.04

TABLE VII. Mass resolution scaling factors s floating within Gaussian constraints in the fits.

Hadron	s
$\Sigma_c(2455)^{++}$	0.93 ± 0.17
$\Sigma_c(2455)^0$	1.07 ± 0.13
$\Sigma_c(2520)^{++}$	1.02 ± 0.20
$\Sigma_c(2520)^0$	1.00 ± 0.20
$\Lambda_c(2595)^+$	0.95 ± 0.15

B. Momentum scale

The accuracy of the momentum scale depends on the precision with which the magnetic field and the amount of material in the detector are known. Both effects are originally calibrated using $J/\psi \rightarrow \mu^+\mu^-$ decays [41]. A limitation of this calibration is that it uses muons that are required by the detector acceptance to have

$p_T > 1.5$ GeV/c, while pions from Σ_c or Λ_c^{*+} decays typically have much lower p_T. The estimate of the uncertainty on the mass differences comes from our previous work on the $X(3872)$ hadron [42]. There, $\psi(2S) \rightarrow J/\psi \pi^+\pi^-$ decays are used to study the momentum scale uncertainties

by comparing the measured $\psi(2S)$ mass with the world average value [26]. In addition, we study the $\psi(2S)$ mass dependence on the kinematic properties of the pions, which constrains the sizes of possible effects. Furthermore, we verify the momentum scale by using $D^*(2010)^+ \rightarrow D^0\pi^+$ decays, where the resulting deviation from the world average is far below the uncertainty derived from $\psi(2S)$. Based on Ref. [42], we assign a 0.12 MeV/c^2 uncertainty on the mass differences of all states under study due to the imperfect knowledge of the momentum scale. The corresponding effect on the natural widths was studied in our previous measurements of the masses and widths of the excited charmed meson states D_1^0 and D_2^{*0} [43], and we

assign the 0.2 MeV/c^2 found there as the uncertainty on the natural widths due to this source. To translate this uncertainty to the coupling constant h_2, we assign it to the sum $\Gamma(\Lambda_c^+ \pi^+ \pi^-) + \Gamma(\Lambda_c^+ \pi^0 \pi^0)$ (see Eqs. (8) and (9)), which is a function of h_2, and perform Gaussian error propagation.

C. Fit model

In terms of our fit model and procedure we check two effects, the internal consistency of the fit and the shape of the signal PDFs. We do not perform an explicit check of the background parametrizations as those are described by polynomials and any analytic function can be approximated by a polynomial of sufficient complexity. Since the fit quality does not indicate significant discrepancies between data and the model, we conclude that the degree of the polynomial functions used is sufficient. Some backgrounds are determined from independent sources, but as the appropriate parameters are Gaussian constrained in the fit, the uncertainty originating from the sample size of the external sources, like Λ_c^+ mass sidebands, is already included in the statistical uncertainties of the results.

To check the internal consistency of the fit procedure, we generate a large ensemble of statistical trials using PDFs of our fit model with parameters obtained from the fit to data. Estimates of all physics parameters except the mass differences and natural widths of the $\Sigma_c(2520)$ resonances are found to be unbiased. The $\Sigma_c(2520)$ mass differences have small biases towards higher values and the $\Sigma_c(2520)$ natural widths are biased towards lower values. These biases on the $\Sigma_c(2520)$ resonance parameters result from the fairly low signal to background ratio and the flexibility in the background PDF, which tends to absorb the tails of the relatively broad signal structure. We repeat the study with a true value for the $\Sigma_c(2520)$ natural width below ($\Gamma = 7.5$ MeV/c^2) and above ($\Gamma = 20$ MeV/c^2) the measured value and find that the biases have a small dependence on the true value. The biases are largest for a true value of the natural width of 20 MeV/c^2 and we consequently assign these biases as systematic uncertainties on the mass differences and natural widths of the $\Sigma_c(2520)$ states.

Concerning the uncertainty on the signal shape, we check whether our signal parametrization using nonrelativistic Breit-Wigner functions provides a proper description. We refit the Σ_c and $\Lambda_c(2625)^+$ data using a *P*-wave relativistic Breit-Wigner function of the form

$$\frac{dN}{dm} \propto \frac{m \cdot \Gamma(m)}{(m_0^2 - m^2)^2 + m_0^2 \cdot \Gamma^2(m)} \quad (14)$$

with

$$\Gamma(m) = \Gamma_0 \left(\frac{q}{q_0}\right)^3 \left(\frac{m_0}{m}\right)\left(\frac{1 + q_0^2 R^2}{1 + q^2 R^2}\right), \quad (15)$$

where $m = \Delta M + m_{\Lambda_c^+}$, R is the Blatt-Weisskopf radius set to 3 (GeV/c)$^{-1}$ [44,45], m_0 and Γ_0 are the nominal mass and width, and $q(q_0)$ is the momentum of the daughters in the Σ_c or $\Lambda_c(2625)^+$ rest frame calculated from the nominal mass. For the $\Lambda_c(2595)^+$ we replace the nonrelativistic Breit-Wigner function of Eq. (7) by a relativistic one and use the variable width defined in Eqs. (8) and (9). For the $\Sigma_c(2455)$ we observe a difference of 0.02 MeV/c^2 in the mass difference, which we assign as a systematic uncertainty. In the cases of $\Sigma_c(2520)$ and Λ_c^{*+} resonances we do not observe any shift and conclude that the effect is negligible.

D. External inputs

Finally, the line shape of the $\Lambda_c(2595)^+$ depends on the input values of the $\Sigma_c(2455)$ masses and widths and the pion decay constant f_π. We repeat the fit using values of those parameters smaller or larger by 1 standard deviation and take the stronger variation as systematic uncertainty. The effect of the uncertainty on the world average $\Sigma_c(2455)$ masses and widths used as input is dominant compared to the effect of the uncertainty on f_π.

VII. RESULTS AND CONCLUSIONS

We perform fits to the $M(pK^-\pi^+\pi^+) - M(pK^-\pi^+)$, $M(pK^-\pi^+\pi^-) - M(pK^-\pi^+)$, and $M(pK^-\pi^+\pi^+\pi^-) - M(pK^-\pi^+)$ mass difference distributions to obtain the desired resonance properties. The data distributions and fits are shown in Figs. 7 and 11. We select about 13 800 $\Sigma_c(2455)^{++}$, 15 900 $\Sigma_c(2455)^0$, 8800 $\Sigma_c(2520)^{++}$, 9000 $\Sigma_c(2520)^0$, 3500 $\Lambda_c(2595)^+$, and 6200 $\Lambda_c(2625)^+$ signal events. The resonance parameters obtained can be found in Table VIII. For the width of the $\Lambda_c(2625)^+$ we observe a value consistent with zero and therefore calculate an upper limit using a Bayesian approach with a uniform prior restricted to positive values. At the 90% credibility level we obtain $\Gamma(\Lambda_c(2625)^+) < 0.97$ MeV/c^2. For easier comparison to previous results [22,25], h_2^2 corresponds to a $\Lambda_c(2595)^+$ decay width of $\Gamma(\Lambda_c(2595)^+) = 2.59 \pm 0.30 \pm 0.47$ MeV/c^2, calculated at $\Delta M(\Lambda_c(2595)^+)$. Our precise measurement of the coupling constant h_2 can, for instance, be used to predict the width of the $\Xi_c(2645)$, as discussed in Ref. [46].

TABLE VIII. Measured resonance parameters, where the first uncertainty is statistical and the second is systematic.

Hadron	ΔM [MeV/c^2]	Γ [MeV/c^2]
$\Sigma_c(2455)^{++}$	$167.44 \pm 0.04 \pm 0.12$	$2.34 \pm 0.13 \pm 0.45$
$\Sigma_c(2455)^0$	$167.28 \pm 0.03 \pm 0.12$	$1.65 \pm 0.11 \pm 0.49$
$\Sigma_c(2520)^{++}$	$230.73 \pm 0.56 \pm 0.16$	$15.03 \pm 2.12 \pm 1.36$
$\Sigma_c(2520)^0$	$232.88 \pm 0.43 \pm 0.16$	$12.51 \pm 1.82 \pm 1.37$
$\Lambda_c(2595)^+$	$305.79 \pm 0.14 \pm 0.20$	$h_2^2 = 0.36 \pm 0.04 \pm 0.07$
$\Lambda_c(2625)^+$	$341.65 \pm 0.04 \pm 0.12$	

In Figs. 13–15, our results are compared to previous measurements by other experiments. Except for $\Delta M(\Lambda_c(2595)^+)$, all our measurements agree with the previous world average values. For $\Delta M(\Lambda_c(2595)^+)$ we show that a mass-independent natural width does not describe the data (see Fig. 12) and observe a value which is 3.1 MeV/c^2 smaller than the existing world average. This difference is the same size as estimated in Ref. [27].

Since this data sample is 25 times larger than the ones studied so far, our results on the properties of Λ_c^{*+} states provide a significant improvement in precision compared to previous measurements. The precision for the Σ_c states is comparable to the precision of the world averages. Concerning the inconsistency of the two CLEO measurements [20,21] of the $\Sigma_c(2520)^{++}$ mass, our data favor a smaller value.
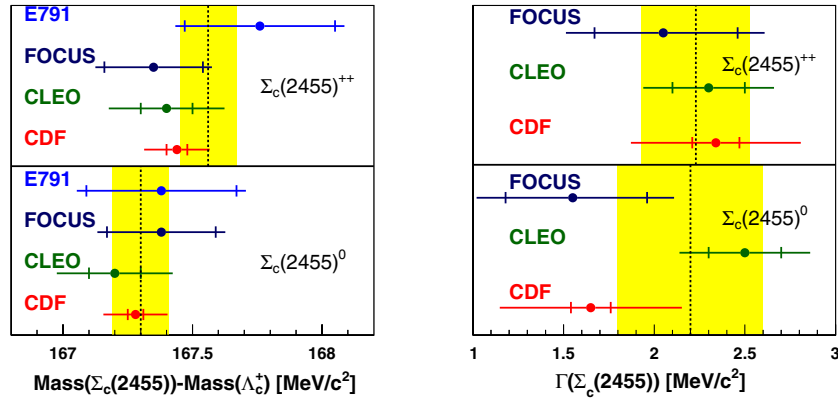
FIG. 13 (color online).   Comparison of our results for the $\Sigma_c(2455)$ mass differences and decay widths with previous measurements by Fermilab E791 [47], FOCUS [19], and CLEO [18]. The error bars represent the statistical (vertical marks) as well as the combined statistical and systematic uncertainties. The vertical dashed line together with the surrounding box symbolizes the world average value and its uncertainty taken from Ref. [26]. This average does not take into account the measurement at hand.
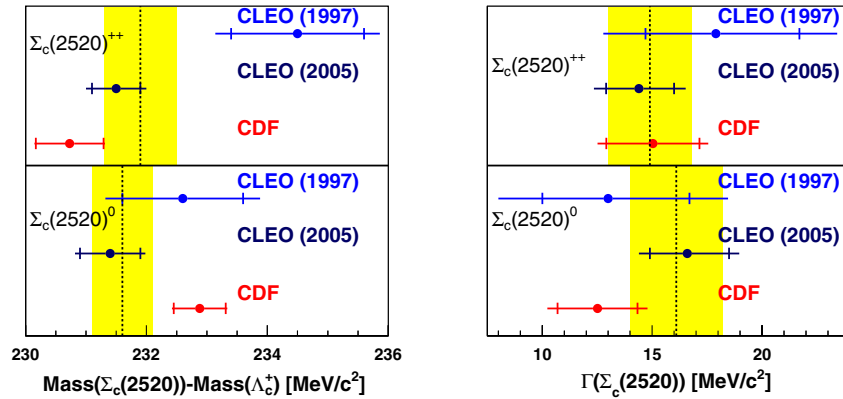

FIG. 14 (color online).   Comparison of our results for the $\Sigma_c(2520)$ mass differences and decay widths with previous measurements by CLEO [20,21]. Further explanations can be found in the caption of Fig. 13.
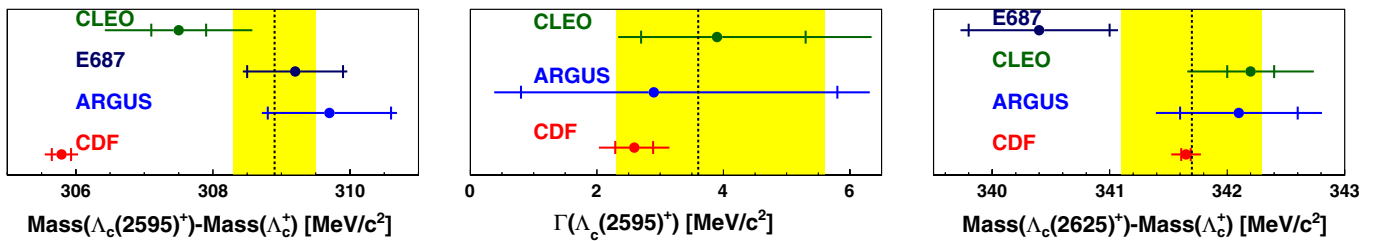

FIG. 15 (color online).   Comparison of our results for the $\Lambda_c(2595)^+$ mass difference and decay width as well as the $\Lambda_c(2625)^+$ mass difference with previous measurements by CLEO [25], Fermilab E687 [23,24], and ARGUS [22]. Further explanations can be found in the caption of Fig. 13.

TABLE IX. Results for the masses and widths of the charmed baryons under study. The first uncertainty is the combined statistical and systematic experimental uncertainty. For the masses, the second uncertainty originates from the world average Λ_c^+ mass [26].

Hadron	M [MeV/c^2]	Γ [MeV/c^2]
$\Sigma_c(2455)^{++}$	$2453.90 \pm 0.13 \pm 0.14$	2.34 ± 0.47
$\Sigma_c(2455)^0$	$2453.74 \pm 0.12 \pm 0.14$	1.65 ± 0.50
$\Sigma_c(2520)^{++}$	$2517.19 \pm 0.46 \pm 0.14$	15.03 ± 2.52
$\Sigma_c(2520)^0$	$2519.34 \pm 0.58 \pm 0.14$	12.51 ± 2.28
$\Lambda_c(2595)^+$	$2592.25 \pm 0.24 \pm 0.14$	$h_2^2 = 0.36 \pm 0.08$
$\Lambda_c(2625)^+$	$2628.11 \pm 0.13 \pm 0.14$	<0.97 at 90% C.L.

In conclusion, we exploit the world largest samples of excited charmed baryons to measure the resonance parameters of six states, namely $\Sigma_c(2455)^{++}$, $\Sigma_c(2455)^0$, $\Sigma_c(2520)^{++}$, $\Sigma_c(2520)^0$, $\Lambda_c(2595)^+$, and $\Lambda_c(2625)^+$. Table IX summarizes the results for their masses and widths. These measurements provide a significant improvement in the knowledge of the resonance parameters of the states and represent the first analysis of charmed baryons at a hadron collider.

[1] D. J. Gross and F. Wilczek, Phys. Rev. Lett. **30**, 1343 (1973).

[2] H. D. Politzer, Phys. Rev. Lett. **30**, 1346 (1973).

[3] T. Mannel, W. Roberts, and Z. Ryzak, Nucl. Phys. **B355**, 38 (1991).

[4] D. B. Lichtenberg, W. Namgung, E. Predazzi, and J. G. Wills, Phys. Rev. Lett. **48**, 1653 (1982).

[5] T. Onogi, arXiv:0906.2344.

[6] N. Mathur, R. Lewis, and R. M. Woloshyn, Phys. Rev. D **66**, 014502 (2002).

[7] W. Roberts and M. Pervin, Int. J. Mod. Phys. A **23**, 2817 (2008).

[8] D. Ebert, R. N. Faustov, and V. O. Galkin, Phys. Lett. B **659**, 612 (2008).

[9] D. Ebert, R. N. Faustov, and V. O. Galkin, Phys. Rev. D **72**, 034026 (2005).

[10] J.-R. Zhang and M.-Q. Huang, Phys. Rev. D **78**, 094015 (2008).

[11] A. Bernotas and V. Simonis, Lithuanian Physics Journal **49**, 19 (2009).

[12] M. A. Ivanov, J. G. Körner, V. E. Lyubovitskij, and A. G. Rusetsky, Phys. Lett. B **442**, 435 (1998).

[13] M. A. Ivanov, J. G. Körner, V. E. Lyubovitskij, and A. G. Rusetsky, Phys. Rev. D **60**, 094002 (1999).

[14] S. Tawfiq, P. J. O'Donnell, and J. G. Körner, Phys. Rev. D **58**, 054010 (1998).

[15] M.-Q. Huang, Y.-B. Dai, and C.-S. Huang, Phys. Rev. D **52**, 3986 (1995).

[16] D. Pirjol and T.-M. Yan, Phys. Rev. D **56**, 5483 (1997).

[17] J. L. Rosner, Phys. Rev. D **52**, 6461 (1995).

[18] M. Artuso *et al.* (CLEO Collaboration), Phys. Rev. D **65**, 071101 (2002).

[19] J. M. Link *et al.* (FOCUS Collaboration), Phys. Lett. B **525**, 205 (2002).

[20] G. Brandenburg *et al.* (CLEO Collaboration), Phys. Rev. Lett. **78**, 2304 (1997).

[21] S. B. Athar *et al.* (CLEO Collaboration), Phys. Rev. D **71**, 051101 (2005).

[22] H. Albrecht *et al.* (ARGUS Collaboration), Phys. Lett. B **402**, 207 (1997).

[23] P. L. Frabetti *et al.* (E687 Collaboration), Phys. Rev. Lett. **72**, 961 (1994).

[24] P. L. Frabetti *et al.* (E687 Collaboration), Phys. Lett. B **365**, 461 (1996).

[25] K. W. Edwards *et al.* (CLEO Collaboration), Phys. Rev. Lett. **74**, 3331 (1995).

[26] K. Nakamura *et al.* (Particle Data Group), J. Phys. G **37**, 075021 (2010).

[27] A. E. Blechman, A. F. Falk, D. Pirjol, and J. M. Yelton, Phys. Rev. D **67**, 074033 (2003).

[28] D. Acosta *et al.* (CDF Collaboration), Phys. Rev. D **71**, 032001 (2005).

[29] C. S. Hill (CDF Collaboration), Nucl. Instrum. Methods Phys. Res., Sect. A **530**, 1 (2004).

[30] A. A. Affolder *et al.* (CDF Collaboration), Nucl. Instrum. Methods Phys. Res., Sect. A **526**, 249 (2004).

[31] D. Acosta *et al.* (CDF Collaboration), Nucl. Instrum. Methods Phys. Res., Sect. A **518**, 605 (2004).

[32] E. J. Thomson *et al.*, IEEE Trans. Nucl. Sci. **49**, 1063 (2002).

[33] L. Ristori and G. Punzi, Annu. Rev. Nucl. Part. Sci. **60**, 595 (2010).

[34] D. J. Lange, Nucl. Instrum. Methods Phys. Res., Sect. A **462**, 152 (2001).

[35] M. Feindt, arXiv:physics/0402093.

[36] M. Feindt and U. Kerzel, Nucl. Instrum. Methods Phys. Res., Sect. A **559**, 190 (2006).

[37] M. Pivk and F. R. Le Diberder, Nucl. Instrum. Methods Phys. Res., Sect. A **555**, 356 (2005).

[38] M. Pivk, arXiv:physics/0602023.

[39] P. L. Cho, Phys. Rev. D **50**, 3295 (1994).

[40] E. Follana, C. Davies, G. Lepage, and J. Shigemitsu (HPQCD and UKQCD Collaborations), Phys. Rev. Lett. **100**, 062002 (2008).

[41] D. Acosta *et al.* (CDF Collaboration), Phys. Rev. Lett. **96**, 202001 (2006).

[42] T. Aaltonen *et al.* (CDF Collaboration), Phys. Rev. Lett. **103**, 152001 (2009).

[43] A. Abulencia *et al.* (CDF Collaboration), Phys. Rev. D **73**, 051104 (2006).

[44] D. Aston *et al.*, Nucl. Phys. **B296**, 493 (1988).

[45] S. Godfrey and N. Isgur, Phys. Rev. D **32**, 189 (1985).

[46] G. Chiladze and A. F. Falk, Phys. Rev. D **56**, R6738 (1997).

[47] E. M. Aitala *et al.* (E791 Collaboration), Phys. Lett. B **379**, 292 (1996).